Rockfall trajectory modeling combined with heuristic analysis for assessing the rockfall hazard along the Maratea SS18 coastal road (Basilicata, Southern Italy)

Roberta Pellicani, Giuseppe Spilotro & Cees J. Van Westen

Landslides
Journal of the International Consortium on Landslides

ISSN 1612-510X

Landslides
DOI 10.1007/s10346-015-0665-3

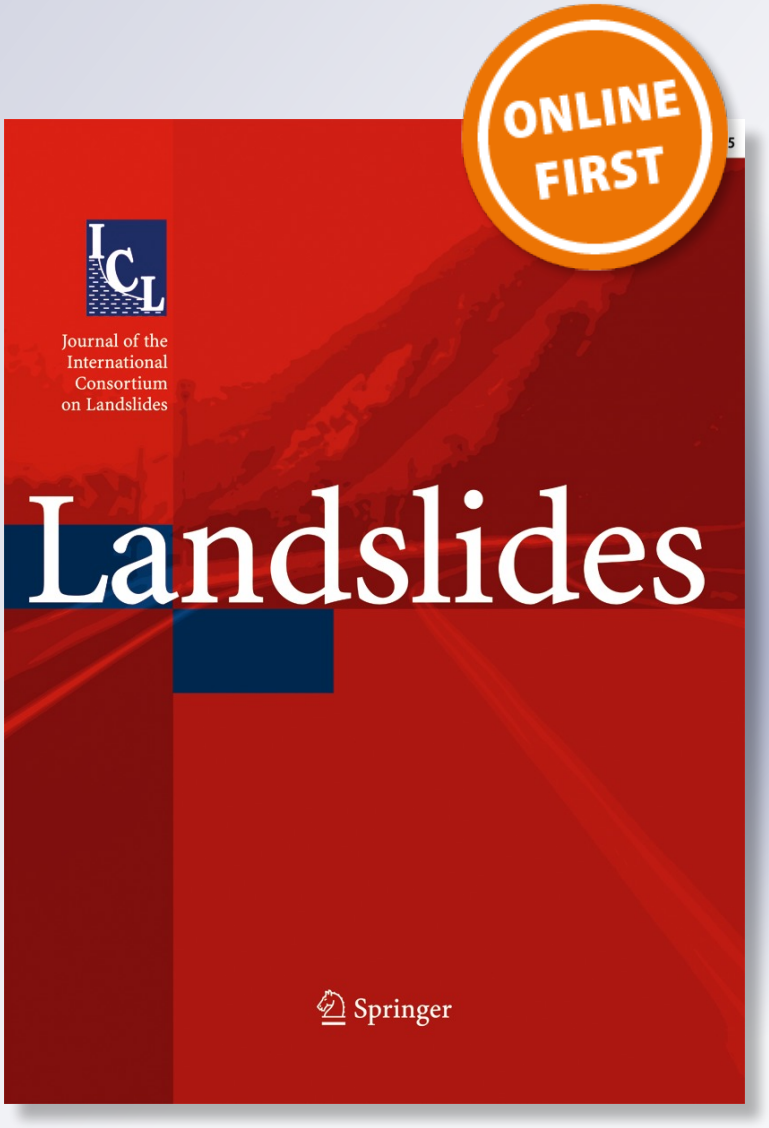

Springer

Original Paper

Landslides
DOI 10.1007/s10346-015-0665-3
Received: 21 May 2015
Accepted: 23 November 2015

Roberta Pellicani · Giuseppe Spilotro · Cees J. Van Westen

Rockfall trajectory modeling combined with heuristic analysis for assessing the rockfall hazard along the Maratea SS18 coastal road (Basilicata, Southern Italy)

Abstract In this paper, a study aimed to assess the rockfall hazard along a portion of the SS18 coastal road, located in the coastal area of Maratea (Basilicata Region, Southern Italy), is presented. The relevance of this study derives from the location of the study area, because the SS18 is a strategic roads in a touristic area, and, since the hazard assessment was performed in 2004 within a project financed by the Viability Regional Department of Autonomous National Company of Roads (ANAS), from the possibility to validate the results by using real rockfall events occurred after 2004. The procedure for assessing the rockfall hazard was composed of four sequential analyses: (i) geomechanical and kinematic characterization of rock mass, (ii) implementation of Romana's (1985) Slope Mass Rating (SMR) method for identifying the potential boulder release areas (rockfall initiation areas), (iii) determination of rockfall trajectories by using a 3D numerical model (ROTOMAP), (iv) calculation and mapping of the hazard index by combining three factors, i.e., (a) lithological features of outcropping materials on rock faces, (b) kinematic compatibility defined by simulating the rockfall trajectories, and (c) spatial distribution of occurred rockfall events. Finally, the proposed methodology was validated by combining the distribution of the hazard levels along the road with the location on the SS18 of the rockfall events occurred from 2004 to 2014.

Keywords Rockfall · Hazard · Trajectory simulation · Coastal road · Protective measures · Heuristic index-based model

Introduction

Rockfall phenomena are widespread in mountain areas with rock cliffs, and in some of these areas, they may cause damage to built-up areas and human lives. This may be particularly so along roads in coastal mountainous areas, with frequent steep cliffs along the transportation corridors, which threaten vehicles and passengers. These coastal roads are often the unique connecting between coastal urban areas, due to the lack of alternative inland roads. Therefore, the rockfall hazard and risk assessment of the coastal transportation corridors, as a basis for planning risk reduction measures, has a crucial importance.

Quantifying the rockfall risk is a complex task, because it involves numerous variables, which are not so easy to determine. In literature, a number of procedures for assessing rockfall risk along roads have been proposed (Pantelidis 2011; Volkwein et al. 2011; Turner and Schuster 2013).

In the recent literature, quantitative risk assessment (QRA) procedures have been developed (Corominas et al. 2005; Pantelidis 2011; Ferlisi et al. 2012; Mignelli et al. 2012; Stock et al. 2012). These methods attempt to estimate the risk in terms of annual probability of loss of property value or life. These approaches calculate the probability that one or more vehicles are impacted, crash against blocks on the road, and use data on the average number of vehicles/day, and their velocity, the frequency of rockfall events of a given magnitude, the vulnerability of passengers, and several other parameters. These methods are affected by uncertainties and simplifications (Pantelidis 2011; Wang et al. 2013). regarding for example the distribution of traffic, the geological characteristics of slopes, etc. One of the major difficulties in rockfall risk assessment is the validation of the resulting risk values.

Procedures for assessing the spatial probability of both rockfall initiation and run-out are widely used, also in combination with GIS spatial analyses (Cancelli and Crosta 1993; Dorren and Seijmonsbergen 2003; Guzzetti et al. 2004; Frattini et al. 2008; Yilmaz et al. 2008; Topal et al. 2012). Numerical calculation codes (2D or 3D) are utilized to simulate the trajectories of boulders down a slope and to assess the probability of different rockfall trajectories (Pfeiffer and Bowen 1989; Guzzetti et al. 2002; Agliardi and Crosta 2003; Stoffel et al. 2006; Agliardi et al. 2009; De Almeida and Kullberg 2011). This kind of models requires detailed information on the materials and corresponding friction and energy restitution coefficients. The validity of these models depends on the representation of the physical phenomena which characterize the rockfall process (free falling, impact, failure with generation of debris, rebound, rolling, and sliding) and on the reliability of input parameters.

The most known procedure for assessing rockfall hazard and risk along roads is the Rockfall Hazard Rating System (RHRS), which is a qualitative method (Pierson et al. 1990; Pierson and Van Vickle 1993). From this method, a series of other systems were derived (Franklin and Senior 1997; Budetta and Panico 2002; Baillifard et al. 2003; Maeez and Youssef 2004; Pack et al. 2006; Mauldon et al. 2007; Russel et al. 2008; Youssef and Maerz 2012). It provides a rating of the risk, by assigning a score to several factors, such as slope geometry, average vehicles risk, magnitude of failure, roadway width, geological character, quantity of rockfall events, climate, and rockfall history. A common characteristic of these systems is the lack of emphasis on the geology and geomorphology of slopes (Budetta 2004; Pantelidis 2011). For this reason, sometimes, these methods are integrated with rock mass classification systems (Romana 1985; Bieniawski 1989; Anbalagan 1992) which allow to take into account the conditions of the rock mass (Budetta 2004). including lithological characteristics and discontinuity data.

This paper presents a procedure to assess, and validate, the rockfall hazard along a portion of the coastal road SS 18 "Tirrena Inferione," running along the Tirrenian coast of Basilicata region (Southern Italy), from 220+600 km to 243+670 km. The study was carried out in two different temporal phases. The rockfall hazard

Published online: 09 December 2015

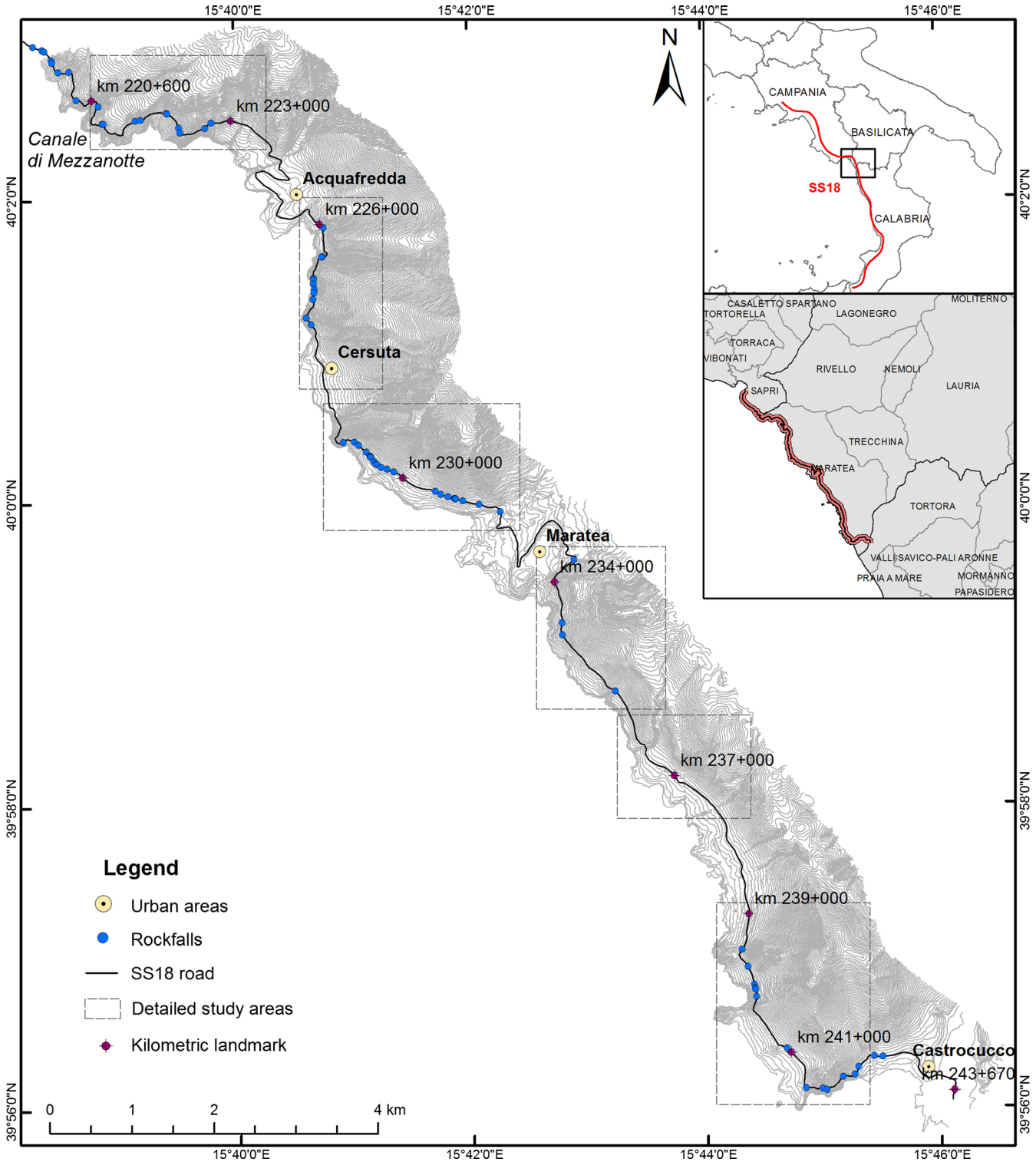

Fig. 1 Study area, SS18 coastal road between 220+600 km and 243+670 km, and location on the road of the blocks deriving from the rockfall events occurred from 1986 to 2003

assessment was performed in 2004 within a project financed by the Viability Regional Department of the Autonomous National Road Company (ANAS) as a basis to design appropriate mitigation measures. The second phase was to validate the results of the hazard model using the rockfall events that occurred from 2004 to 2014.

The procedure for the rockfall hazard assessment was carried out in three subsequent steps. First, a heuristic slope instability assessment system, using the Slope Mass Rating (SMR) model (Romana 1985; Budetta 2004; Gupta and Tandon 2014). has been applied in order to individuate the most unstable areas on the rock slopes bordering the road, which are potential rockfall

Fig. 2 Photos of steep and fractured rock slopes overhanging the SS18 coastal road (**a**) and rockfall on the road (**b**)

detachment areas. Then, a three-dimensional model, ROTOMAP (Geo and Soft International 2004). has been used to simulate the rockfall trajectories, starting from the initiation areas previously determined, and to assess the probability of impact points of blocks along the road. Finally, an index-based approach for assessing and mapping rockfall hazard along the road was carried out. The hazard index was defined as a simple combination of three factors: (a) lithological features of outcropping materials on rock faces, (b) kinematic compatibility defined through the fall trajectories and (c) spatial distribution of historical rockfall events.

The 3D modeling of rockfall trajectories aimed also to verify the technical efficiency and suitability of the existing defensive measures. On the basis of the spatial distribution of rockfall hazard, resulting from the 2004 project, appropriate protection measures have been designed for the road stretches subjected at higher hazard (Colangelo and Guariglia 2011). These protective measures are important because the SS18 is a strategic road in a touristic area and it was studied much less than similar tourist roads, such as the Amalfi and Sorrento coastal roads (Budetta 2004; Calcaterra et al. 2004; Ferlisi et al. 2012). The study along the SS18 also allows to validate the results by using real rockfall events, which occurred after 2004.

The Maratea SS18 coastal road

Geological and geomorphological setting

The SS18 "Tirrena Inferiore" is an important infrastructure, which connects three regions in Southern Italy: Campania, Basilicata, and Calabria. It runs along the Tirrenian coast for 535 km, of which a stretch of 23 km in the Basilicata area was analyzed in this study, between 220+600 km and 243+670 km, passing through the territory of Maratea and connecting the urban areas of Castrocucco, Maratea, Cersuta, and Acquafredda. This stretch extends a rugged part of the coastline, between the "Canale di Mezzanotte" in the North and Castrocucco in the South near the outlet of the Noce River (Fig. 1).

In this area, the slopes overhanging the coastal road are characterized by vertical or sub-vertical rock faces, with various systems of discontinuities (Fig. 2a), many of which are open and often karstified. There are also many signs of ancient rockfall phenomena and many scree slopes.

The main geological formations, outcropping in the coastal slopes, belong to the structural-stratigraphical units of the "Campano-Lucana" Platform and "Liguridi" units (D'Argenio et al. 1973; Cotecchia et al. 1990), characterized by a calcareous-dolomitic sequences.

The current geomorphological setting of the area is the result of Plio-Quaternary tectonic activity that caused numerous faults. The most important tectonic element in the study area is the Sapri-Rivello-Seluci fault, which has a northern sector (near Mt. Serralunga) characterized by monoclinal structures directed NW-SE and a southern sector (near Mt. Coccovello and Mt. Lauria) characterized by structures directed W-E.

In the northern part of the study area (from 220+600 km to Acquafredda), the coastline is characterized by massive sub-vertical cliffs (up to 100 m). Acquafredda is located on a torrential fan, partly terraced and bordered at the sea side, by high cliffs. In the stretch between Acquafredda and Cersuta, steep coastal slopes, characterized by morphological concavities filled with coarse detrital deposits both loose and cemented, are present. Cersuta is also located on a partially terraced debris deposit. The road runs, from Cersuta to Maratea, along the seashore at the bottom of sub-vertical rock slopes and at the top of re-profiled slopes, with stretches characterized by incisions and ancient debris deposits. The valley of Maratea has widespread outcrops of talus deposits. The southern part of the study area, from Maratea to Castrocucco, is almost entirely composed by dolomite sequences, belonging to the Mt. Bulgheria-Verbicaro Unit, tectonically overlain on limestones, belonging to the Alburno-Cervati Unit, with intercalations of clayey and marly units. The slopes, facing the sea, follow a fault scarp due to the straight and parallel nature, accompanied by the production of detrital deposits.

The study area has a hydrogeological relevance due to the presence of three different hydro-structures (i.e., Mt. Coccovello-Mt. La Serra, Mt. Crivo and Mt. Rotonda-Serra di Castrocucco) and is characterized by periodic heavy rainfall events.

Rockfall events before 2004

The instability phenomena affecting the rock slopes overlying the road occur periodically during abundant rainfalls, freeze-and-thaw cycles, earthquakes, etc. and constitute a significant risk for the road and for the vehicles. For the hazard assessment, a rockfall database containing the events that affected the coastal

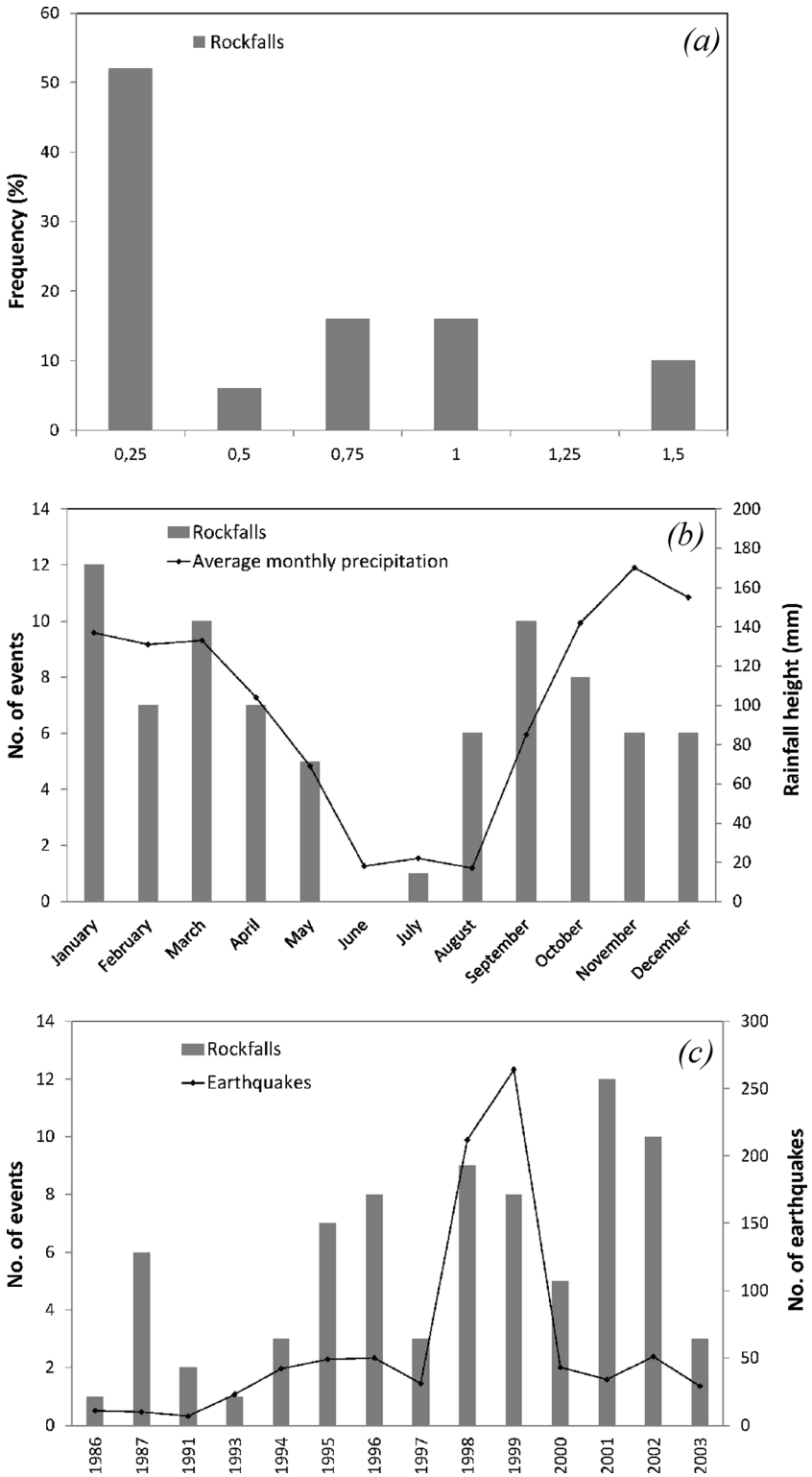

Fig. 3 Statistical distributions of the rockfall events occurred from 1986 to 2003: **a** frequency-block volume classes, **b** monthly distribution of rockfalls compared with the average monthly distribution of rainfalls, **c** annual distribution of rockfalls compared with the annual distribution of earthquakes

road from 1986 to 2003 was prepared by collecting the information recorded by the Civil Protection Department of Basilicata Region and ANAS (Viability Regional Department of the Autonomous National Road Company). In particular, seventy-eight rockfall events, of which seventy reached the road and eight were intercepted by protective barriers, were collected (Fig. 2b). The database contains, for a given rockfall event, information on the date of occurrence, the spatial localization of the deposition area on the road (in terms of kilometric landmarks) and the size of boulders. The last information is not available for all the events

Table 1 Values of adjustment factors: F_1, F_2, and F_3 in relation to joint and slope orientation and for different failure modes; F_4 for different methods of excavation (Romana 1985; Spilotro et al. 2004)

Adjustment factors		Orientation classes				
Failure modes		Very favorable (very low failure probability)	Favorable	Fair	Unfavorable	Very unfavorable (very high failure probability)
P/W	$\lvert\alpha_{j/i}-\alpha_s\rvert$	>30°	30°–20°	20°–10°	10°–5°	<5°
T	$\lvert\alpha_j-\alpha_s-180\rvert$					
	F_1	0.15	0.40	0.70	0.85	1.00
P/W	$\beta_{j/i}$	<20°	20°–30°	30°–35°	35°–45°	>45°
T	β_j					
	(P/W) F_2	0.15	0.40	0.70	0.85	1.00
	(T) F_2	1.00	1.00	1.00	1.00	1.00
P/W	$\lvert\beta_{j/i}-\beta_s\rvert$	>10°	10°–0°	0°	0–(−10°)	<−10°
T	$\lvert\beta_{j/i}+\beta_s\rvert$	<110°	110°–120°	>120°	–	–
	F_3	0	−6	−25	−50	−60
	F_4	Natural slopes	Presplitting	Smooth blasting	Blasting or mech. excavation	Deficient blasting
		15	**10**	**8**	**0**	**−8**

P planar sliding, *W* wedge sliding, *T* toppling, α_s dip direction of slope, $\alpha_{j/i}$ dip direction of joint or intersection line of two joints, β_s dip of slope, $\beta_{j/i}$ dip of joint or intersection line of two joints

contained in the database but only for the 30 % of them. For this sample of events, statistical evaluation of the volumes of the fallen blocks, which range from 0.04 to 1.5 m^3, was carried out in order to obtain a characteristic distribution of volume classes. As shown in Fig. 3a, the distribution has a frequency maximum for smallest block ($V<0.3$ m^3) and rapidly decreases for greater volumes.

Information on the triggering factors and the consequences (damage to vehicles or to the road, accidents, etc.) was not contained in the database. As shown in Fig. 1, the events are mostly concentrated in the central-northern part of the study area and in a limited stretch of the SS18 immediately at North of Castrocucco.

The monthly and annual distributions of the rockfall phenomena were determined. The first was compared with the distributions of average monthly precipitations, obtained from the meteorological station of Maratea from 1986 to 2001. While the second was compared with the annual distribution of earthquakes, extracted from the historical catalogue of National Institute of Geophysics and Volcanology (INGV). The monthly distribution (Fig. 3b) shows that the rockfalls are essentially concentrated in January, when rainfalls are most intense and the minimum temperature is lowest, and in March and October, which are the most rainy months in spring and autumn. The annual distribution of rockfall events (Fig. 3c) is characterized by two peaks: the first is in the period 1998–1999, the second and more intense is in the period 2001–2002. This trend could be correlated with the seismic activity of the area. During 1998 and 1999, about 470 small earthquakes with magnitude between 3.4 and 5.3 occurred at a distance up to 35 km from Maratea (Rizzo and Leggeri 2004; INGV 2010). The correlation between rockfalls and seismic events is less evident in the period 2001–2002, when the local seismic activity was more weak, with earthquake magnitudes up to about 3.5. However, these comparisons between (monthly and annual) rockfall frequencies and temporal distribution of triggering factors did not provide a quantitative correlation that could be used in establishing threshold values.

Procedure for rockfall hazard assessment

The procedure performed earlier in the 2004 project (Spilotro et al. 2004) for assessing the rockfall hazard along the coastal road SS18 was composed of four sequential analyses: (i) geomechanical and kinematic characterization of rock masses, (ii) implementation of Romana's (1985) SMR method for identifying the potential boulder release areas (rockfall initiation areas), (iii) determination of rockfall trajectories by using a 3D numerical model (ROTOMAP), (iv) calculation and mapping of the hazard index by combining three factors, i.e., (a) lithological features of outcropping materials on rock faces, (b) kinematic compatibility defined by simulating the rockfall trajectories, and (c) spatial distribution of historical rockfall events. With reference to the portion of the SS18 comprised between 220+600 km and 243+670 km, the rockfall hazard assessment was carried out only in six areas, due to the lack of information in some other zones of the study area. For example, the geomechanical characterization of rock slopes did not cover the entire area due to the difficulty to survey these data especially near the urban areas. In order to avoid the use of inhomogeneous input data, the analyses were carried out in those areas within which the input data were uniformly distributed.

Table 2 Description of the SMR index and stability classes with the corresponding potential failure mode and suggested stabilization measures (Romana 1985)

Class n.	V	IV	III	II	I
SMR values	0–20	21–40	41–60	61–80	81–100
Description	Very bad	Bad	Normal	Good	Very good
Stability	Completely unstable	Unstable	Partially stable	Stable	Completely stable
Failures	Big planar or soil-like or circular	Planar or big wedges	Planar along some joints or many wedges	Some blocks	No failure
Support	Re-excavation	Corrective	Systematic	Occasional	None

Geomechanical surveys and kinematic analyses

During the 2004 project, several geomechanical surveys were carried out in order to classify the rock masses, by using the Rock Mass Rating (RMR) system of Bieniawski (1979, 1989). and to evaluate the potential failure mechanisms, though the Markland's (1972) test, along the studied road stretches. The stability conditions of rock slopes are strongly influenced by the geostructural features of the rock mass. Therefore, a correct evaluation of the trend of discontinuities within the rock mass in relation to the slope orientation is crucial for the identification of falling paths of potentially unstable boulders (Ghosh et al. 2010). For the geomechanical characterization of the rock mass, 150 horizontal (frontal) and 29 vertical scan lines were distributed along the six road stretches. These scan lines covered about 17.2 km in length and 628 m in height. For each outcrop, the orientation properties of discontinuities (dip, dip direction, and strike) were first recognized. Secondly, the following parameters were recorded in the rock mass and along the discontinuities: number of joints families, dip and dip direction of each discontinuities, compressive strength of rock material, Rock Quality Designation (RQD) values, spacing between discontinuities, persistence, roughness and aperture of the joints, type and nature of the filling material, hydraulic conditions, and weathering conditions of discontinuities. These parameters were used for classifying the rock mass by calculating the RMR indexes (Bieniawski 1979, 1989). The geomechanical survey has been executed according to ISRM standards (International Society for Rock Mechanics 1981).

The kinematic analysis has been carried out using the Markland's(1972) test, in order to analyze the potential failure mechanisms. In general, the kinematic analysis, which is purely geometric, examines which modes of failure are possible in a jointed rock mass, without consideration of the forces involved (Gupta and Tandon 2014). The Markland's test differentiates the sliding along one plane (planar sliding) from the sliding along the line of intersection of two joints (wedge sliding) and from the toppling. In particular, angular relationships between discontinuities (dip and dip direction) and slope surfaces (slope angle and aspect) were applied to determine the potential and modes of failures.

Identification of potential rockfall initiation areas by using SMR method

The geomechanical data, i.e., RMR index and joint orientation properties, were used for evaluating the spatial distribution of SMR index (Romana 1985) on the rock slopes overlying the road. The Slope Mass Rating (SMR) system is a heuristic slope instability model, which has been applied in order to individuate the most unstable areas on the rocky slopes overlying the road, which are potential rockfall detachment areas.

The SMR index is generally is obtained, by modifying the RMR index (Bieniawski 1989) through four adjustment factors, three depending on the relationship between joint and slope orientation and one factor related to the excavation method, through the following equation:

$$\mathrm{SMR} = \mathrm{RMR}_{1989} + (F_1 \times F_2 \times F_3) + F_4 \quad (1)$$

where RMR_{1989} is the Rock Mass Rating by Bieniawski (1989). F_1 reflects the parallelism between joint (α_j) and slope (α_s) face strikes. F_2 refers to joint dip angle (β_j) in failure planar mode and the plunge of the intersection line of two discontinuities (β_i) in the failure wedge mode. F_3 reflects the relationship between the dip of joints (β_j) and the slope angle of rock faces (β_s). F_4 is related to the method of slope excavation; for natural slopes, the value of F_4 is 15. In Table 1, the values of adjustment factors F_1, F_2, and F_3 for different failure modes (planar sliding, wedge sliding, and toppling) are listed. The SMR index ranges between 0 and 100 and is subdivided into five classes of instability (Table 2). In order to obtain a spatial distribution of the most unstable areas on the slopes overlying the road according to the SMR index, the Romana's model was performed in GIS through the following steps: (a) Generation of a Digital Terrain Model (DTM) with a spatial resolution of 1 m (1×1-m cell size), by interpolating the contour lines extracted from a topographic map at scale 1:1000. From the DEM, standard morphometric

Table 3 Values of normal (k_n) and tangential (k_t) energy restitution coefficients and dynamic friction coefficient (μ) used to set-up the rockfall trajectory simulations in ROTOMAP

Lithological units	k_n	k_t	μ
Limestone	0.53	0.95	0.40
Loose debris	0.32	0.82	0.65
Cemented breccia	0.35	0.85	0.40
Colluvial deposit	0.30	0.80	0.70
Calcareous conglomerate	0.45	0.90	0.45
Calcarenite-calilutite	0.53	0.95	0.40
Marl	0.40	0.80	0.45
Dolomite	0.53	0.95	0.40

Table 4 Orientation parameters of discontinuity families and intersection lines and corresponding modes of failure resulting from the kinematic analysis (only the intersection joints kinematically compatible with a failure mode are listed here)

Typology	Dip direction [°N]	Dip [°]	Failure mode
S1–S2			
Joint	102	81	Toppling
Joint	110	75	Toppling
Joint	193	79	Planar sliding
Stratification	233	11	–
Joint	325	75	Planar sliding
Intersections	27	59	Toppling
	37	48	Toppling
	153	76	Wedge sliding
	179	52	Wedge sliding
	263	59	Wedge sliding
S3–S4			
Joint	26	79	Toppling
Joint	35	75	Toppling
Joint	105	80	Toppling
Joint	122	83	Toppling
Joint	198	85	Planar sliding
Joint	201	76	Planar sliding
Stratification	224	11	–
Joint	333	78	–
Intersections	14	75	Toppling
	37	65	Toppling
	44	58	Toppling
	58	73	Toppling
	62	77	Toppling
	66	78	Toppling
	96	62	Toppling
	112	40	Toppling
	133	78	Toppling
	149	82	Toppling
	162	72	Wedge sliding
	183	75	Wedge sliding
	265	60	Wedge sliding
	275	69	Wedge sliding
	355	77	Toppling
S5–S6			
Joint	230	51	Toppling
Joint	254	62	Toppling
Joint	293	64	Planar sliding
Joint	11	47	Planar sliding
Joint	82	60	Toppling
Joint	123	39	Planar sliding
Joint	114	87	–
Joint	122	84	Planar sliding

information layers were obtained, i.e., the slope and aspect maps; (b) elaboration of a thematic map of the RMR_{1989} index, by superimposing the geomechanical data on a 1×1-m grid, geographically coherent with DEM; (c) elaboration of thematic maps related to the orientation properties of joints (dip, dip direction, and strike), using a 1×1-m grid; (d) production of thematic maps related to the adjustment factors F_1, F_2, and F_3 by using overlay functions among the maps of joint orientation properties and the maps of slope and aspect of rock faces; (e) elaboration of the SMR index map and, subsequently, the final SMR stability class map, always through overlay functions among the maps of the adjustment factors and the map of the RMR_{1989} index.

On the basis of the SMR index, a spatially distributed classification of unstable areas on the rock slopes has been obtained, taking into account the quality of the rock mass (through the RMR index) and the spatial relationships between the discontinuities and the orientation of the rock faces. These most unstable areas have been considered as potential rockfall detachment areas and used as input release areas for the subsequent numerical simulation of the rockfall trajectories.

Numerical simulation of rockfall trajectories

In order to ascertain the more likely rockfall trajectories, the ROTOMAP software (*Geo&Soft International*), a three-dimensional numerical model for rockfall simulation, was used. ROTOMAP uses a "lumped mass" approach that considers dimensionless boulders with all the mass concentrated in a point, i.e., the center of mass, and requires the following input data (Geo&Soft 2004; Scioldo 2006):

- Digital elevation model (DEM) representing the topographic surface in raster format
- Rockfall source areas, using a grid map indicating the location of the cells from which boulders detach
- Number of starting points, indicating the number of boulders launched from each grid cell and, so, the number of the trajectories computed from each cell
- Number of initial velocities of boulder, as well as minimum and maximum initial velocity (m/s)
- Number of initial directions and maximum angular deviation (°)
- Kinematic parameters, i.e., limit angles of flying (starting threshold for free falling after impact), colliding (starting threshold for free falling), and bouncing (free falling/rolling transition threshold after impact)
- Geomechanical parameters of rolling boulders, i.e., normal and tangential energy restitution coefficients and dynamic friction coefficient

Table 5 Rock mass classification (Bieniawski 1979, 1989) of sample fronts belonging to the limestones of Alburno-Cervati Unit (S1, S2, S3, and S4) and the dolomites of Mt. Bulgheria-Verbicaro Unit (S5 and S6) (Spilotro et al. 2004)

Parameters	S1–S4		S5		S6	
	Value	Index	Value	Index	Value	Index
Compressive strength of rock material	80 MPa	7	80 MPa	7	81 MPa	7
RQD	82 %	17	73 %	13	86 %	17
Spacing of joints	260.1 mm	10	175.8 mm	8	310 mm	10
Conditions of joints:						
Persistence	>2 m	4	>2 m	4	>2 m	4
Aperture	1–5 mm	1	1–5 mm	1	>5 mm	0
Roughness	Slightly rough	3	Slightly rough	3	Slightly rough	3
Filling	Hard filling >5 mm	2	Hard filling >5 mm	2	Hard filling >5 mm	2
Weathering conditions	Moderately weathered	3	Moderately weathered	3	Slightly weathered	5
Hydraulic conditions	Completely dry	15	Completely dry	15	Completely dry	15
RMR	**62**		**56**		**63**	

The rockfall trajectories, computed by ROTOMAP, depend on the starting points and the coefficients used to simulate the loss of velocity at the impact point or where the boulder is rolling and take into account the three-dimensional effect of topography, which may cause lateral dispersion of rockfalls. In addition, ROTOMAP provides as output, by using a statistical approach, the probable block arrival areas (or the distribution of spatial frequency of stopping points), the maximum and average kinetic energy, the minimum traveling time, and the rebound height of the blocks. This software enables to design the defensive measures by analyzing the distribution of average and maximum kinetic energy. The first allows to identify the location of these structures in correspondence of relative minimum values; the second provides information on the strength required for them. In addition, the model simulates the interaction between blocks and existing countermeasures by introducing the barrier geometry (height), their energy absorption capacity (strength, kJ), and the boulder mass.

In the 2004 project, the simulations passed through the following main steps: (i) assigning the input parameter values to different lithologies, (ii) defining the topographic surface, (iii) individuating the rockfall detachment areas, and (iv) evaluating the technical suitability and efficiency of the existing defensive measures, especially rockfall barriers.

The normal and tangential energy restitution coefficients and dynamic friction coefficient are generally affected by large variability and uncertainty due to the complexity of the local interactions between boulders and slopes (Guzzetti et al. 2002). depending on the size and shape of boulders, dynamic compressibility of material constituting the slope, geometry of the boulder-slope impact points, etc. Based on field experiments and numerical simulations, some authors (Piteau and Clayton 1978; Barret and Pfeiffer 1989; Pfeiffer and Bowen 1989; Agliardi et al. 2009) evaluated that, for natural slopes, the dynamic friction coefficient (μ) ranges from about 0.30 to 1.0 and the normal (k_n) and tangential (k_t) energy restitution coefficients range, respectively, from 0.20 to 0.50 and between 0.40 and 0.90. In order to define appropriate values of normal and tangential energy restitution coefficients and dynamic friction coefficients to be assigned to the different lithological units, aback-calibration of model was carried out by using a small sample of more recent (occurred in 2003) and well-documented rockfall events. For the back-analysis, the locations of boulders, fallen on the road or stopped by the defensive barriers, were used as stopping points in modeling. The values of the parameters (μ, k_n, k_t) resulting from the calibration are summarized in Table 3. The trajectories were computed by using as three-dimensional topographic surface the DEM with spatial resolution of 1 by 1 m. The rockfall source areas were obtained considering the most unstable areas, according to the SMR classes (classes III, IV, and V), and a number of tracks of scarps, extracted from a geomorphological map at 1:2000 scale.

The analysis of the technical efficiency of defensive measures was carried out in order to determine potential weakness zones, through which the blocks may pass and reach the road. The actual energy absorption capacity of existing rockfall defensive barriers was obtained through a 20 % reduction of their nominal theoretical value, for accounting the reduction of efficiency due to impacts of blocks or to aging.

Finally, nine conditions were simulated, by combining three different values of block volume (0.5, 1, and 10 m^3) and three different values of initial velocity (5, 10, and 20 m/s). The volumes 0.5 and 1 m^3 were chosen according to the frequency distribution of recorded historical rockfall events (Fig. 3a), while 10 m^3 was considered more representative of potential extreme events. This value was taken into account also for representing those events in which the initial block, which detaches from the rock slope, breaks

Fig. 4 Map showing the distribution of the SMR stability classes along the rock slopes overhanging the SS18 and graphs synthesizing the morphometric features of the hillslopes affected by the SMR stability classification: **a** frequency distribution of the mean aspect, **b** frequency distribution of the mean slope angle, **c** minimum, mean and maximum values of elevation

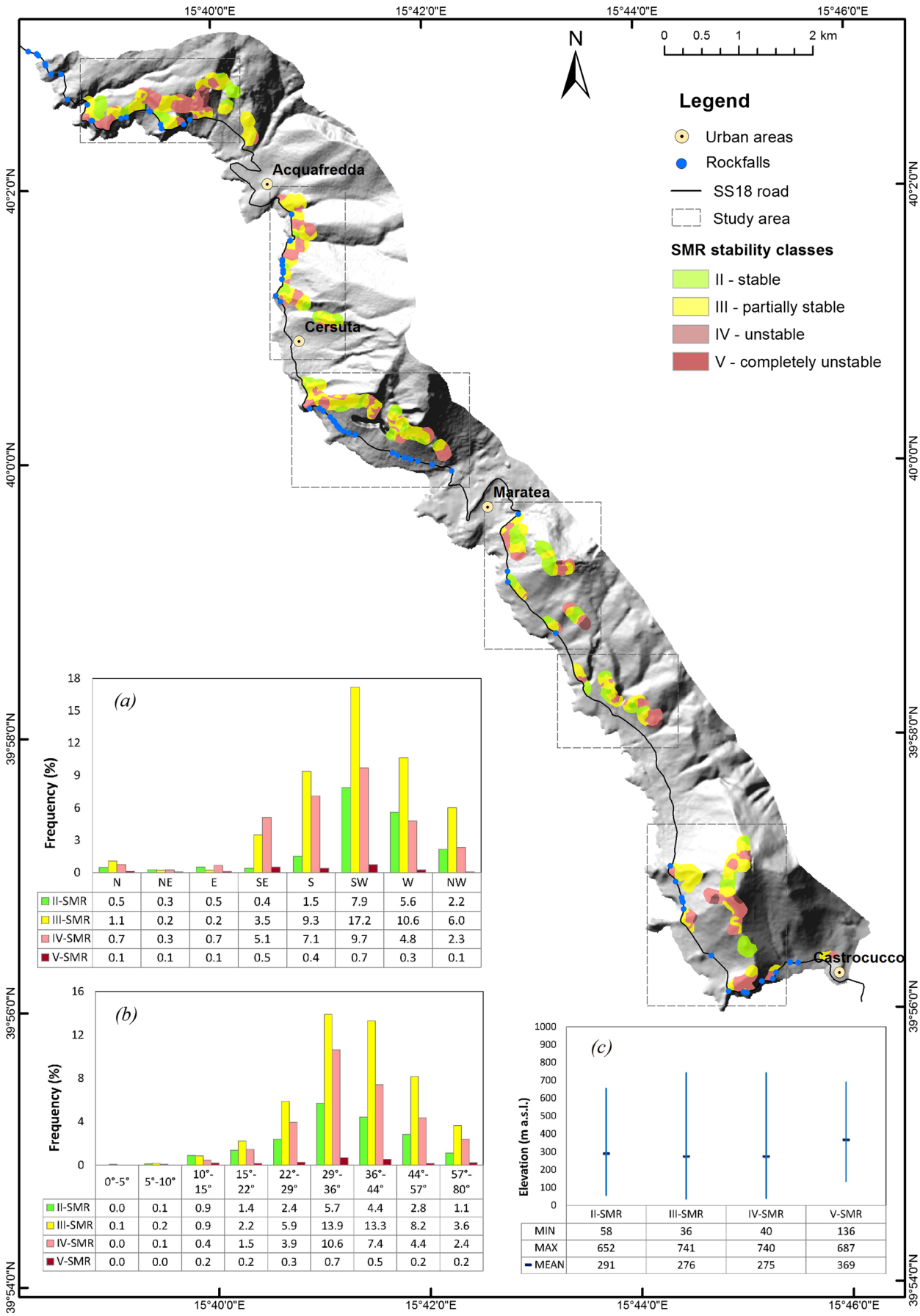

(a)

Frequency (%)

	N	NE	E	SE	S	SW	W	NW
II-SMR	0.5	0.3	0.5	0.4	1.5	7.9	5.6	2.2
III-SMR	1.1	0.2	0.2	3.5	9.3	17.2	10.6	6.0
IV-SMR	0.7	0.3	0.7	5.1	7.1	9.7	4.8	2.3
V-SMR	0.1	0.1	0.1	0.5	0.4	0.7	0.3	0.1

(b)

Frequency (%)

	0°-5°	5°-10°	10°-15°	15°-22°	22°-29°	29°-36°	36°-44°	44°-57°	57°-80°
II-SMR	0.0	0.1	0.9	1.4	2.4	5.7	4.4	2.8	1.1
III-SMR	0.1	0.2	0.9	2.2	5.9	13.9	13.3	8.2	3.6
IV-SMR	0.0	0.1	0.4	1.5	3.9	10.6	7.4	4.4	2.4
V-SMR	0.0	0.0	0.2	0.2	0.3	0.7	0.5	0.2	0.2

(c)

Elevation (m a.s.l.)

	II-SMR	III-SMR	IV-SMR	V-SMR
MIN	58	36	40	136
MAX	652	741	740	687
MEAN	291	276	275	369

itself during the rolling along the slope, producing several smaller blocks, which accumulate on the road.

Rockfall hazard assessment

The general definition of risk (Varnes 1984) is generally expressed in probabilistic terms (Glade et al. 2005) and requires the analysis of the probability of occurrence of a rockfall event with a given magnitude, the probability that a block reaches the element at risk, vulnerability, and economic value of elements at risk (Mavrouli and Corominas 2010). These risk components depend on a large number of factors, for example, the probability of occurrence depends on the rockfall frequency-magnitude relationship and triggering event frequencies, the reaching probability on the propagation process along the slope and mobility of element at risk, the vulnerability depends on rockfall intensity, and characteristics of exposed assets (Corominas et al. 2005; Agliardi et al. 2009; Ferlisi et al. 2012, Wang et al. 2013). As often there are not enough data to make a reliable assessment of these quantities (Pellicani et al. 2014a). the procedure for evaluating the rockfall risk, in quantitative terms, is affected by large uncertainty (Wang et al. 2013). For this reason, in absence of detailed data, the spatial distribution of rockfall hazard along the SS18 road was assessed using a qualitative index-based approach. It assumed that the rockfall hazard, H_{rf}, was a simple combination of three parameters, through the following expression:

$$H_{rf} = L \times T_{rf} + C_{rf} \quad (2)$$

Where L represents the outcropping lithological units on rock faces, T_{rf} represents the kinematic compatibility defined by simulating the rockfall trajectories, and C_{rf} represents the spatial distribution (or count) of historical rockfall events. Although the heuristic models are often characterized by simplifications, they provide results equally reliable than those produced by quantitative methods (Pellicani et al. 2014b).

The lithological outcrops on the rock faces overlying the road were considered as the main predisposing factor of rockfall phenomena. The highly susceptible areas were assumed coinciding with the most rockfall-prone lithological units, such as, for example, the landslide debris deposits, representing the tracks of past rockfall events, or the outcrops tectonically disturbed and fractured.

The T_{rf} factor was obtained from the numerical modeling of rockfall trajectories, by evaluating the distribution of probable arrival points of blocks on the road. This term was computed subdividing the road into stretches of 50 m length and evaluating three different scenarios: (1) the blocks do not reach the road, (2) the blocks reach the road but the frequency (or probability) of arrival point on the road is low, (3) the blocks reach the road but the frequency (or probability) of arrival point on the road is high. This factor provides indirectly information on the expected frequency of rockfall occurrence; the larger the number of computed trajectories, the higher the expected frequency of rockfall occurrence. In addition, it takes into account intrinsically the spatial distribution of the zones more unstable, individuated by SMR method, and so potentially affected by block detachments.

The historical rockfall events along a given road stretch were considered an important witness of the stability conditions of slopes. C_{rf} was expressed as a dichotomous variable, assuming a 0 value if a given road stretch was not affected by past rockfalls and a 1 value if past events occurred. It should be highlighted that, although C_{rf} was defined in a cell, representing the road, it was extended to the right and left buffer zones (10 m each) of the cell. This approximation had the aim of extending information associated to a single rockfall event, whose location was probably recorded (in the inventory) in correspondence of the largest block, to a stretch large enough to account the "swarm" fall of smaller blocks.

The thematic maps, corresponding to the above-mentioned hazard factors, were reclassified assigning a score to each class, according to its influence on the rockfall process. The three reclassified maps were overlaid, implementing the hazard index algorithm, and rockfall hazard values were obtained in each grid cell. The final rockfall hazard map was obtained, reclassifying each road stretch into three classes, with low, medium, and high hazard level.

Fig. 5 Location of rockfall protection measures in each study area and corresponding graph showing the percent ratio of the length of a given type of measure to the total length of the measures in that study area (*A*) and the percent ratio of the length of a given type of measure to the total length of that type along the 23 km of the SS18 (*B*). Legend of typologies of rockfall countermeasures: (*a*) fixed drapery double twisted wire mesh, (*b*) surficial reinforcing revetment nets, (*c*) rockfall catch fences with high energy absorption level, (*d*) surficial reinforcing panels, (*e*) rockfall catch fences with medium energy absorption level, (*f*) rockfall catch fences with low energy absorption level]

Results and discussion

Application of the rockfall hazard procedure

The geomechanical characterization of the rock masses was carried out on 151 horizontal and 29 vertical scan lines distributed along the SS18 road, with a total number of 1033 and 192 measurements, respectively. Along each scan line, the main families of joints and their orientation were recognized. A mean of seven families per front, with a maximum number of 24 and a minimum of 1, were surveyed. Since it would be difficult to show all the 1225 measurements, only the results of surveys carried out along the more representative fronts, belonging to the two geolithological units, i.e., limestones of Alburno-Cervati Unit and dolomites of Mt. Bulgheria-Verbicaro Unit, are presented here. For the first unit, four scan lines (S1, S2, S3, and S4) along rock faces characterized by a high frequency of past rockfalls and a high number of discontinuity families were selected. For the second one, two scan lines (S5 and S6) were chosen in correspondence of a stretch of rock slopes with a low number of discontinuity families and low frequency of past rockfalls. In total number, 147 joints were identified, whose orientation was analyzed by means of stereographic projections (Smith equal-area and Wulff equal-angle stereonets). From the pole density stereo-plots, the main families of discontinuities were individuated (Table 4). For each of them and for the intersection lines of two discontinuities, the kinematic analysis was carried out through the Markland's (1972) test and the failure modes were determined (Table 4): toppling and planar sliding for the discontinuities, toppling and wedge sliding for the intersection lines. Finally, the geomechanical characterization of the rock mass, by using the Rock Mass Rating (RMR) system of Bieniawski (1989).

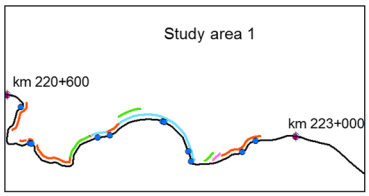

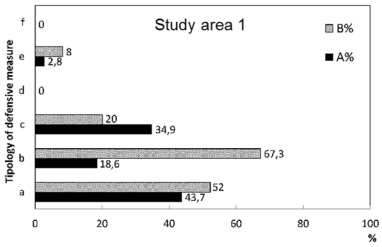

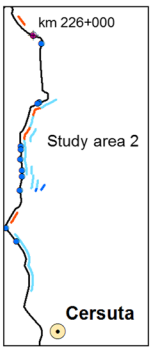

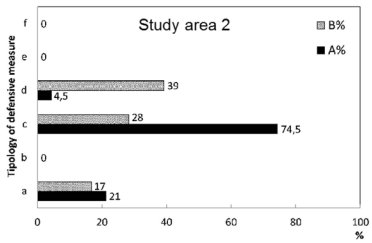

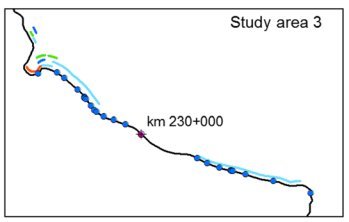

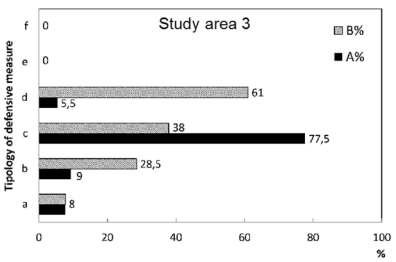

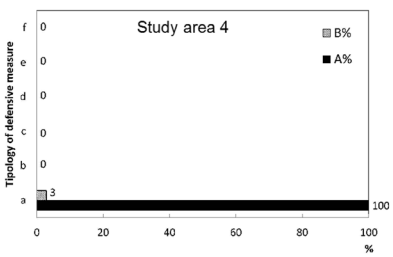

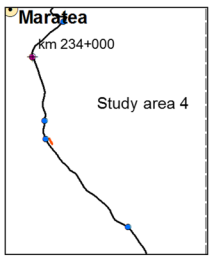

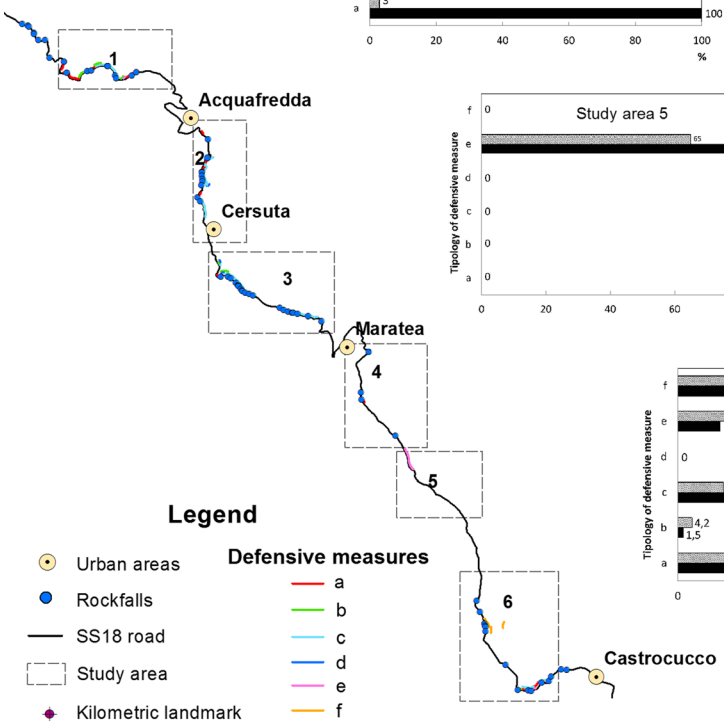

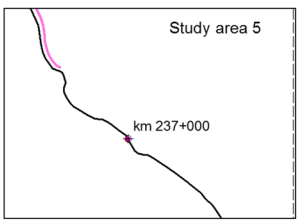

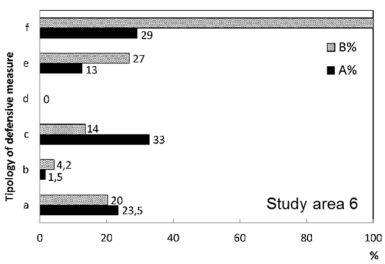

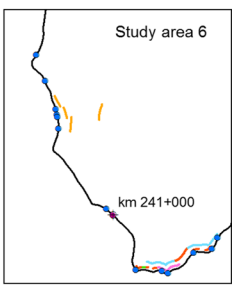

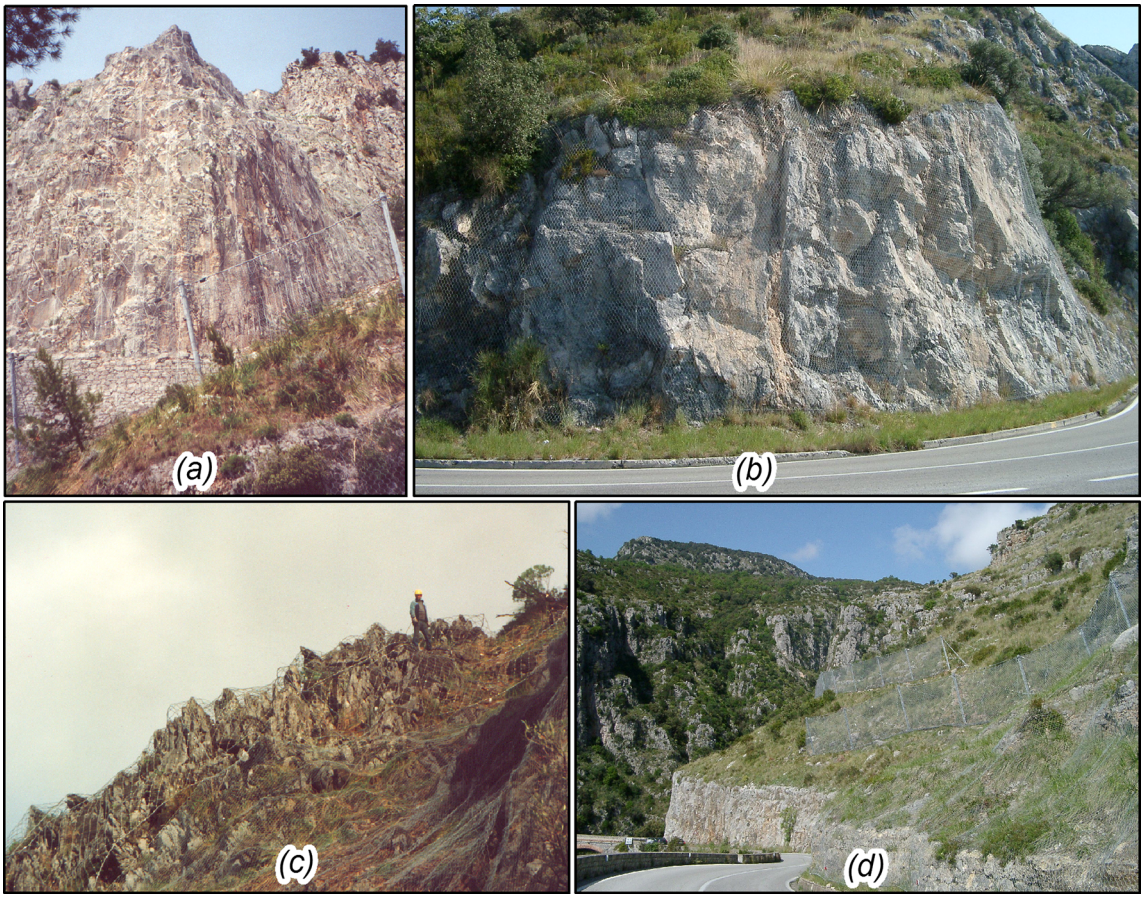

Fig. 6 Examples of defensive measures distributed along the SS18 in 2004: **a** surficial reinforcing revetment nets, **b** fixed drapery double twisted wire mesh, **c** surficial reinforcing panels, **d** rockfall catch fences

was performed. Mean values of the rock mass and joints parameters, needed for determining RMR values and relative to S1-S4, S5, and S6 scan lines, are shown in Table 5. The joints have moderate apertures (1–5 and >5 mm), with medium spacing (260, 176, and 300 mm) and low-medium persistence (>2 m). The joints are slightly rough, filled with hard fine material and moderately to slightly weathered. Finally, the hydraulic conditions of rock masses are not significant and most of the joints are dry. According to RMR values, i.e., 62 for the scan lines from S1 to S4, 56 for S5, and 63 for S6, the rock mass in the selected sample lithological units was classified as good (S1-S4 and S6) and discrete (S5) rock.

The geomechanical data, RMR indexes and joint orientation parameters, were mapped in GIS, using a 1×1-m grid (coherent with the DTM spatial resolution), in order to obtain, according to the procedure described in the paragraph 3.2, the thematic maps related to the adjustment factors F_1, F_2, and F_3 and to the SMR index (Romana 1985). The map in Fig. 4 shows the spatial distribution of the stability classes, obtained by ranking the SMR index according to Table 2. Analyzing the SMR class map, it emerges that the stability class I completely stable is not present, the partially stable areas (class III) cover the 48 % of the overall area classified trough the SMR index, followed by the unstable (31 %), stable (19 %), and completely unstable (2 %) areas. The morphometric analysis of the hillslopes affected by the SMR mapping reveals that they are mainly south-west faced (Fig. 4a), with a lower percentage

Table 6 Results of 300 ROTOMAP simulations for each combination block volume-initial velocity, expressed in terms of number of times in which the blocks exceed the barriers

	V_{block} [m^3]	V_{start} 5 m/s	V_{start} 10 m/s	V_{start} 20 m/s
Area 1	0.5	5	3	7
	1	8	6	18
	10	58	78	89
Area 2	0.5	2	4	6
	1	4	7	11
	10	32	50	68
Area 3	0.5	0	0	2
	1	6	8	14
	10	42	46	50
Area 5	0.5	0	0	0
	1	0	0	1
	10	8	9	12
Area 6	0.5	13	14	14
	1	39	41	45
	10	50	55	69

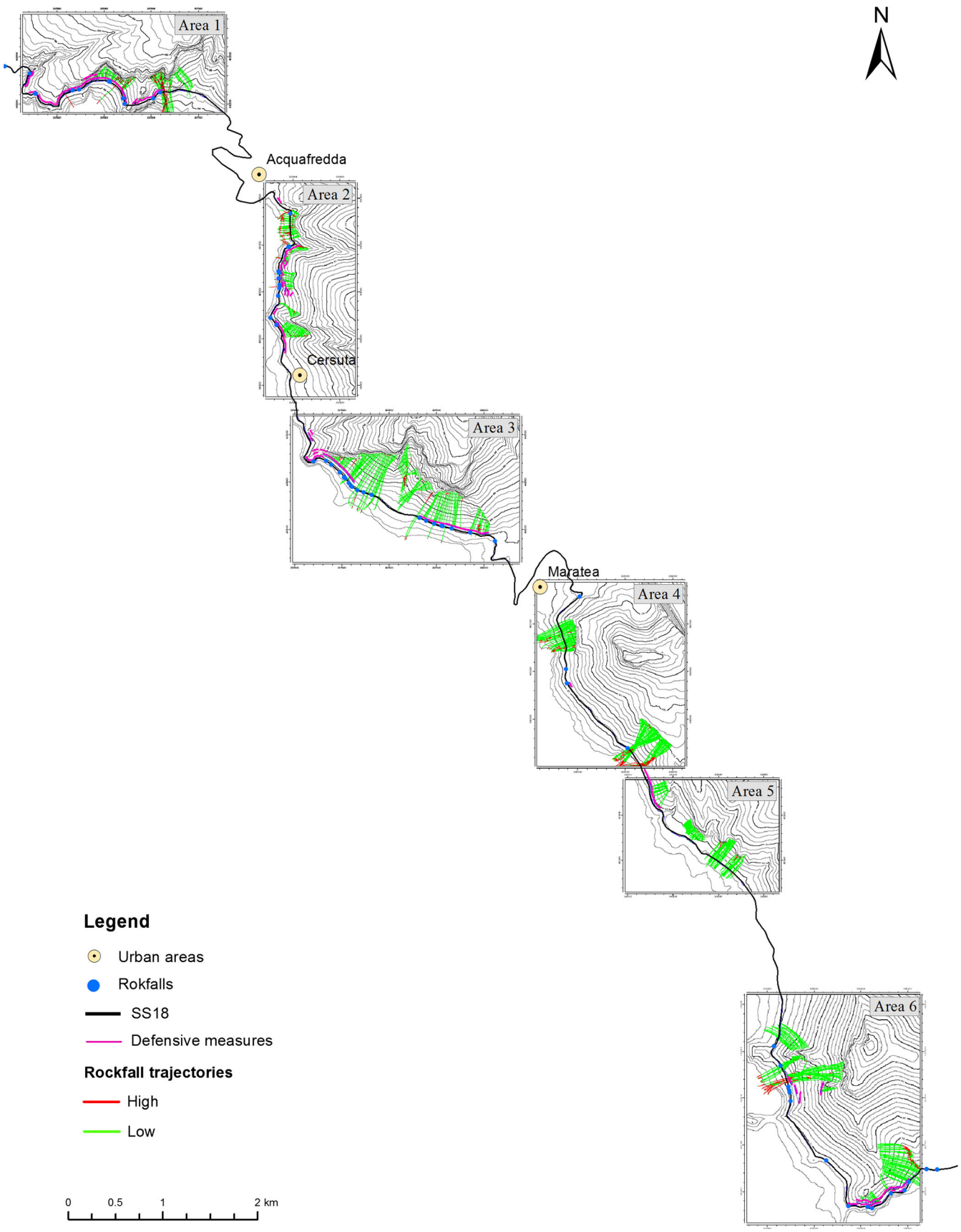

Fig. 7 Simulated rockfall trajectories in the six study areas, classified by different probability of stopping of blocks: high if more than 50 boulders reach the road (*red lines*) and low if less than 50 boulders reach the road (*green lines*)

Table 7 Classes and relative scores used for reclassifying the thematic maps of the three hazard factors: lithology (L), rockfall trajectories (T_{rf}), and past rockfall events (C_{rf})

Factor	Class	Score	Description
Lithology (L)	1	1	Debris cone, fan, detrital deposits
	2	0.8	Limestones, brecciated limestones, dolomites
	3	0.6	Conglomerates
	4	0.4	Conglomerates with marls and argillites
	5	0	Alluvial covers
Rockfall trajectories (T_{rf})	1	1	Blocks reach the road with high probability (N_{block}>50)
	2	0.5	Blocks reach the road with low probability (N_{block}<50)
	3	0	Blocks do not reach the road
Rockfall events (C_{rf})	1	0	The road stretch is not affected by past rockfalls
	2	1	The road stretch is affected by past rockfalls

south and west faced, and their mean slope angle ranges between 36° and 44° (Fig. 4b), with minimum and maximum values of, respectively, 10° and 80°. Finally, the potentially most unstable areas (class V) are characterized by high elevation values and relative relief lower than the other areas, since the minimum altitude is greater than the others (Fig. 4c), about 136 m a.s.l.

The simulations of the potential rockfall trajectories were performed using the input data listed in paragraph 3.3 and considering nine combinations of block volumes (V_b=0.5, 1, and 10 m^3) and initial velocities (v_s=5, 10, and 20 m/s). Among the output data resulting from the trajectory modeling using ROTOMAP, the most important for the aim of this study were the distribution of probable arrival points of blocks on the road, useful for the subsequent hazard assessment, and the evaluation of the effectiveness of the rockfall defense measures.

In particular, four types of rockfall protection measures were distributed along the road in 2004 (Fig. 5): surficial reinforcing revetment nets (Fig. 6a), fixed drapery double twisted wire mesh (Fig. 6b), surficial reinforcing panels consisting of a double twisted wire mesh and high tensile steel ropes (Fig. 6c), and rockfall catch fences with different (low, medium, and high) energy absorption levels (Fig. 6d). The superimposition of the database of rockfalls that occurred from 1986 to 2003 on the distribution of protection measures showed a good spatial match. Indeed, out of 77 recorded events, 8 were intercepted by the barriers, 14 occurred outside the six study areas, and 55 reached the road. Among the last 55 events, 34 were located in correspondence with the existing measures; this revealed a correct positioning of the barriers. In order to evaluate the incidence of the different types of existing measures along the six road stretches, the following percent ratios were computed: (A) percent ratio of the length of a given type of measure in a study area to the total length of the measures in that study area, (B) percent ratio of the length of a given type of measure in a study area to the total length of that type along the 23 km of the SS18. As shown in Fig. 5, the rockfall catch fences with high energy absorption level were the most used, especially in the study areas 2 and 3; the most protected area (62 %) is the area 1, mainly with fixed drapery systems and barriers; the areas 4 and 5 were, respectively, measure-free and poorly protected (12 %). The types of countermeasures less used were surficial reinforcing panels and the rockfall catch fences with low and medium energy absorption level, located almost exclusively in areas 5 and 6.

For evaluating the effectiveness of the rockfall defense measures, 300 simulations were performed in ROTOMAP, for each combination V_b-v_s, and the number of times in which the blocks pass the barriers was computed. The results obtained in the six study areas are summarized in Table 6 and represented in Fig. 7. In area 1, the stretch of SS18 (3 km length) has been partially protected by means of about 2 km of rockfall barriers, which were well located in relation to the occurred rockfall events. However, these measures did not cover the entire front potentially affected by detachments, especially in the upper parts (eastern side of the area). The simulations highlighted a reasonably good reliability of barriers only for initial velocities of 5 and 10 m/s (corresponding to a detachment high up to about 20 m) and for block volumes not greater than 1 m^3. The same results have been obtained for the area 2 and 3. As already mentioned, area 4 was without countermeasure; thus, an analysis was performed considering a block volume of 0.5 m^3 and initial velocity of 5 m/s in order to determine only the stretches of road with a high probability of being reached by blocks detached from the overlaying rock fronts. Along the 2 km of road crossing area 5, the unique protection measure present in 2004 was a rockfall barrier with a nominal absorption strength of 1750 Kj. Although this area was not affected by rockfalls, the trajectory modeling was performed considering the rock faces classified as unstable and completely unstable, according to SMR index, as rockfall source areas. The results of the ROTOMAP simulations showed that the barrier was not adequate to ensure a substantial protection of the road. For area 6, in which 8.6 km of road was protected by means of 1.5 km of countermeasures, the results of the simulations showed a significant decrease of the reliability of rockfall barriers, also for initial velocity of 5 m/s. In general, the analysis of the spatial distribution of the simulated trajectories reveals that the frequency of rockfalls is not uniform along the SS18 road. The trajectories with high probability of occurrence, and a high chance of reaching the road, are mainly concentrated along steep slopes and channels, where debris deposits outcrop.

The final rockfall hazard map was obtained by combining the thematic maps, corresponding to the three already mentioned

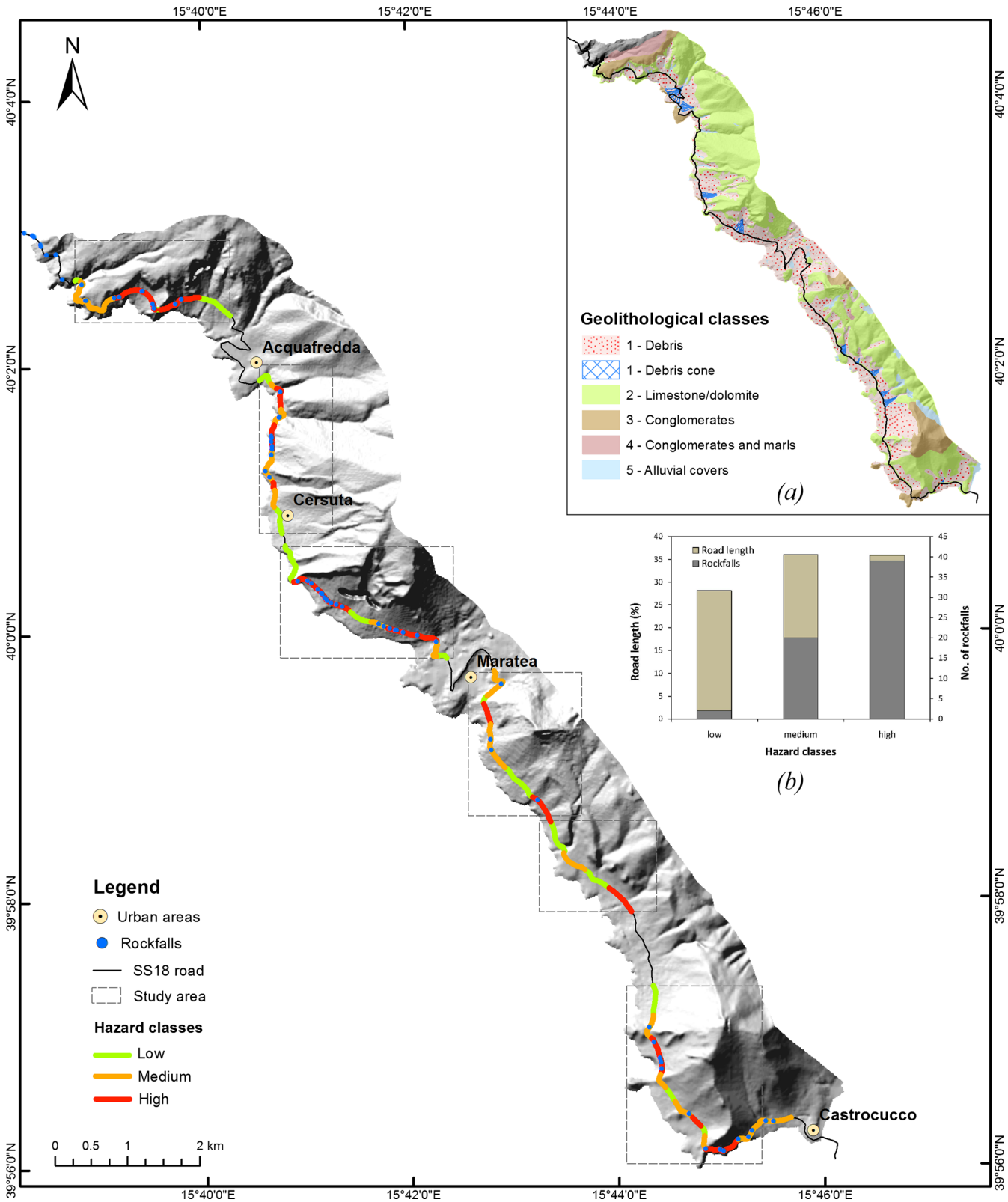

Fig. 8 Rockfall hazard map of the SS18 road ranked into three hazard level (low, medium, and high) with **a** geolithological map subdivided into five lithological classes, **b** graph showing the percentage of the road and the number of rockfalls included in each of the three hazard classes

factors, according to the algorithm shown in paragraph 3.4. Before overlaying, these maps were reclassified and a score was assigned to each class according to its influence on the instability process. The classes and their relative scores are synthetized in Table 7. For the lithological factor, a lithological map of the study area at 1:5000 scale, containing about 24 lithological units, was

Table 8 Hazard classes assigned to each combination of the factor classes, i.e., lithology (L), rockfall trajectories (T_{rf}), and rockfall events (C_{rf})

Hazard factors			Hazard values	Hazard classes	Hazard factors			Hazard values	Hazard classes
L	T_{rf}	C_{rf}			L	T_{rf}	C_{rf}		
1	1	1	2	High	1	1	0	1	Medium
0.8	1	1	1.8	High	0.8	1	0	0.8	Medium
0.6	1	1	1.6	High	0.6	1	0	0.6	Medium
0.4	1	1	1.4	High	0.4	1	0	0.4	Low
0	1	1	1	Medium	0	1	0	0	Low
1	0.5	1	1.5	High	1	0.5	0	0.5	Medium
0.8	0.5	1	1.4	High	0.8	0.5	0	0.4	Low
0.6	0.5	1	1.3	High	0.6	0.5	0	0.3	Low
0.4	0.5	1	1.2	Medium	0.4	0.5	0	0.2	Low
0	0.5	1	1	Medium	0	0.5	0	0	Low
1	0	1	1	Medium	1	0	0	0	Low
0.8	0	1	1	Medium	0.8	0	0	0	Low
0.6	0	1	1	Medium	0.6	0	0	0	Low
0.4	0	1	1	Medium	0.4	0	0	0	Low
0	0	1	1	Medium	0	0	0	0	Low

reclassified by unifying the similar lithologies and assigning a score, ranging from 0 to 1, to the resulting five lithological classes according to their predisposing role in the rockfall process (Fig. 8a). The definition of the scores was heuristic, based on the experience and background knowledge. The highest values were assigned to debris and to limestone and dolomite outcrops, respectively, 1 and 0.8. Intermediate values were awarded to conglomerates (0.6) and conglomerates in clayey and marly matrix (0.4), and, finally, zero value was assigned to alluvial soils, which are completely irrelevant for the rockfall occurrence. For mapping the factor relative to the rockfall trajectories, the SS18 road was subdivided into stretches of 50 m length and the following scores were assigned to them: 1 to the road stretches which had a high probability of being reached by detached blocks (boulders reaching the road more than 50), 0.5 to the road stretches with low probability of being reached (less than 50), and 0 to the road stretches that were not reached by any blocks. As already mentioned, the occurrence of past rockfall events, which affected the road, was considered through a dichotomous variable, assuming 0 value if a given road stretch was not affected by past rockfalls and 1 value if past events occurred. Before assessing and mapping the rockfall hazard, the spatial data contained in the three hazard factor maps were made uniform. The lithological map was overlaid with the SS18 road in vector format, in order to obtain a new thematic map in which the outcropping lithologies were distributed directly on the road linear vector. In the other two thematic maps, the spatial distribution of information was already of a linear type and data were stored in road sections 50 m length. Therefore, each map was transformed into a raster map with the same spatial resolution, i.e., 5×5 m.

By overlaying the rockfall hazard factor maps and implementing the hazard algorithm, the rockfall hazard index values were obtained in each grid cell. These values of the rockfall hazard index did not provide an immediate understanding of the hazard level, especially for the intermediate values which are more difficult to interpret than the extreme values. For this reason, the hazard index values were ranked into the three classes of hazard, low (0–0.4), medium (0.5–1.2), and high (1.3–2), according to the scheme shown in Table 8. Road sections not affected by past rockfall events (C_{rf}=0) and not reached by blocks launched during the simulations (T_{rf}=0) or reached with low probability (T_{rf}=0.5) are characterized by low hazard, regardless of the lithological class. Conversely, the presence of past events (C_{rf}=1) along the road stretches intercepted by simulated rockfall trajectories with low (T_{rf}=0.5) or high (T_{rf}=1) probability involves a high hazard level, except for those sections located on alluvial terrains. A medium level of hazard corresponds to lithological classes predisposing the instability (L=1, 0.8 and 0.6) only whether past events are not present (C_{rf}=0) and the probability of blocks reaching the road is high (T_{rf}=1). A medium level corresponds also to lithological classes not predisposing the instability (L=0.4 and 0) only whether past events are present (C_{rf}=1). The final rockfall hazard map was obtained, reclassifying each road section into the three hazard classes, low, medium, and high (Fig. 8).

Figure 8b shows the percentage of the road and the number of rockfalls included in each of the three hazard classes. The road sections subjected to low rockfall hazard are 28 % (4.9 km) on the total length, while the remaining 72 % (12.4 km) of the examined road stretches is affected, in equal parts, by medium and high hazard levels. The comparison between the hazard map and the location of past events reveals that 63.9 % of rockfalls occurred in sections where the hazard is high and 32.8 % in sections where the hazard is medium. The remaining 3.3 % of rockfalls occurred in road stretches where the hazard is assessed low.

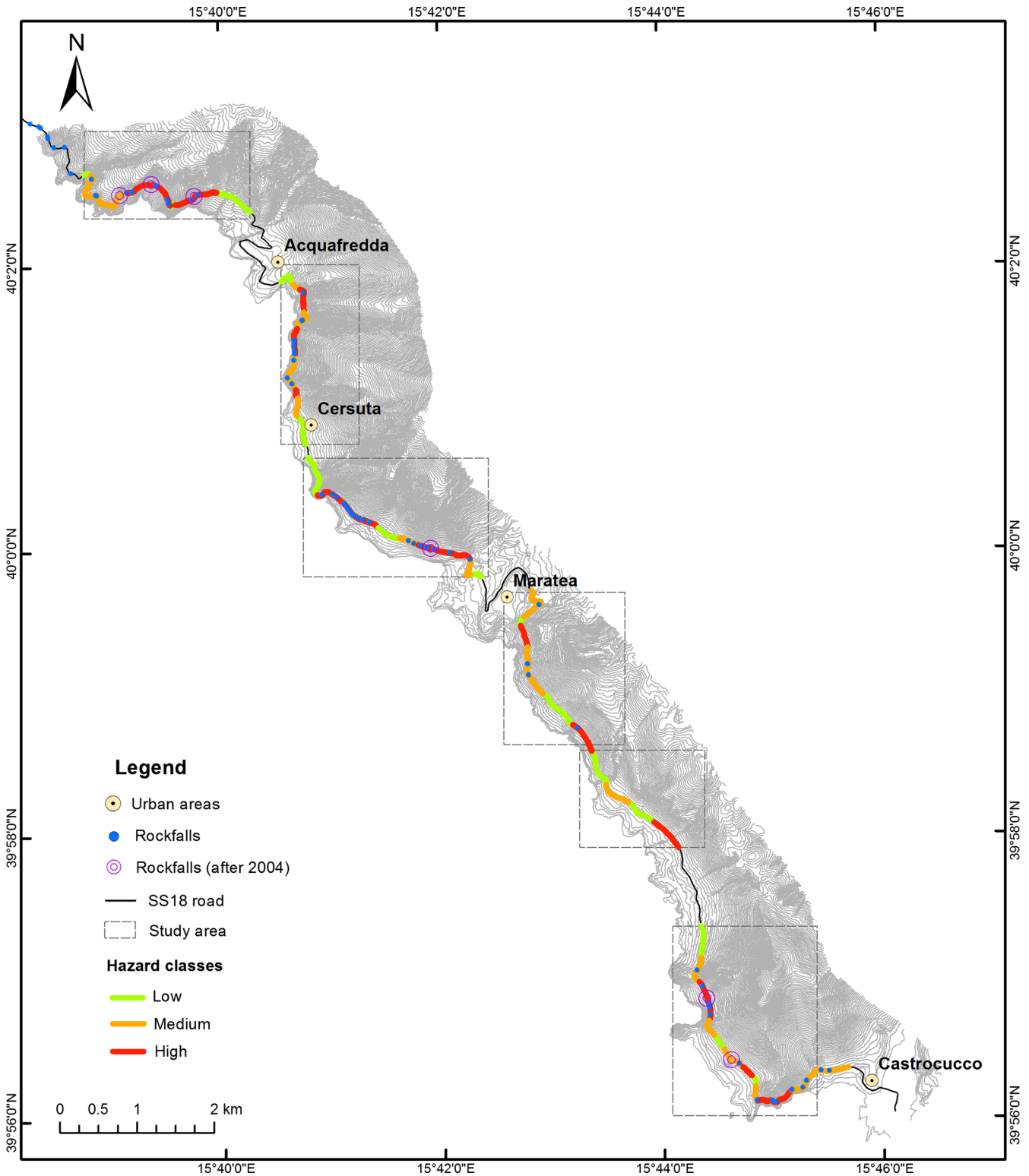

Fig. 9 Spatial overlay between the rockfall hazard map and the location of the rockfall events recorded by the Civil Protection between 2004 and 2014

Validation

The rockfall hazard model, calibrated by using events occurred between 1986 and 2003, was validated by combining the distribution of the hazard levels with the location on the SS18 of the events that occurred from 2004 to 2014. In particular, only six rockfall events were provided by Civil Protection Department of Basilicata Region (Fig. 9). The first two events took place on December 2006 in the southern sector of the examined SS18 road, near Castrocucco, in correspondence of two sections classified at medium and high hazard level. The subsequent two events, occurred

one after three months from the other (September 2009 near Acquafredda and December 2009 in Torre dei Crivi site), took place on road stretches at high and medium hazard, respectively. Finally, the latter two rockfalls, occurred on February 2010 at Rasi site and on November 2014 at north of Acquafredda, have affected two road sections mapped at high hazard. The number of rockfall events after 2003 is too small to validate in quantitative terms the hazard analysis, for example, by using the success-rate curves or ROC curves, etc. However, the qualitative spatial validation, carried out by overlaying the hazard distribution and the location of the deposition area on the road of the more recent rockfall events, has highlighted reliable performance and a good predictive capability of the proposed methodology.

It should be noted that even if the rockfall events collected by Civil Protection after 2003 are not probably all those actually occurred, in the last 10 years, the number of rockfalls has been lower than the number of events occurred in the previous 17 years, due to the efficiency of the protective fences, designed by Civil Protection as a result of the hazard analysis carried out in 2004.

Conclusions

The study herein presented has showed a procedure, worked out in 2004, for assessing and mapping the rockfall hazard along the coastal SS18 road, in order to provide useful indications to local governments for improving the mitigation measures already present along the road. The specificity of this methodology resides in the use of the rockfall events subsequently occurred, from 2004 to 2014, for validating the rockfall hazard map.

The procedure proposed for assessing and mapping the rockfall hazard is composed of four sequential analyses: (i) geomechanical and kinematic characterization of rock mass, (ii) implementation of Romana's (1985) SMR method for identifying the potential boulder release areas (rockfall initiation areas), (iii) determination of rockfall trajectories by using a 3D numerical model (ROTOMAP), (iv) calculation and mapping of the hazard index.

This procedure, although is based on a combined analysis of data on rockfall deposition locations, on lithological, structural, topographical, and geomorphological features of the slopes overhanging the road, and on the geomechanical properties of rock mass, has provided a reliable estimation of rockfall hazard. The choice to implement a qualitative heuristic index-based approach, which allows to calculate the rockfall hazard as a simple combination of three parameters, i.e., lithological features of outcropping materials on rock faces (L), kinematic compatibility defined by simulating the rockfall trajectories (T_{rf}), and spatial distribution of occurred rockfall events (C_{rf}), derives from the absence of detailed input data. The quantitative calculation of the hazard and risk, as defined by Varnes (1984) and generally expressed in probabilistic terms, requires the analysis of the probability of occurrence of a rockfall event with a given magnitude, the probability that a block reaches the element at risk, the vulnerability, and the economic value of elements at risk. These components depend on a large number of factors, for example, the rockfall frequency-magnitude relationship, the run-out of the detached boulders along the slope, the characteristics of elements at risk (static or moving assets), etc. In the absence of reliable data on these factors, a hazard and risk analysis would have been affected by large uncertainties.

Finally, the procedure validation, carried out by overlaying the hazard distribution and the localization of the deposition area on the road of the rockfall events occurred between 2004 and 2014, has highlighted reliable performance and a good predictive capability of the proposed methodology. This is an important result, as it shows that it is possible to use, for the rockfall hazard assessment, a simplified procedure based on data easy to find and manage.

Acknowledgments

The Authors are grateful to Antonio Petraglia (consultant geologist) for his assistance in carrying out the geomechanical surveys and Gerardo Colangelo (Civil Protection of Basilicata) for providing data on recent rockfall events.

References

Agliardi F, Crosta G (2003) High resolution three-dimensional numerical modelling of rockfalls. Int J Rock Mech Min Sci 40:455–471

Agliardi F, Crosta GB, Frattini P (2009) Integrating rockfall risk assessment and countermeasure design by 3D modeling techniques. Nat Hazards Earth Syst Sci 9(4):1059–1073

Anbalagan R (1992) Landslide hazard evaluation and zonation mapping in mountainous terrain. Eng Geol 32:269–277

Baillifard F, Jaboyedoff M, Sartori M (2003) Rockfall hazard mapping along a mountainous road in CH using a GIS-based parameter rating approach. Nat Hazards Earth Syst Sci 3:431–438

Barret RK, Pfeiffer T (1989) Rockfall modeling and attenuator testing. US Department of Transportation, Federal Highway Administration, Final Report, 107 pp

Bieniawski ZT (1979) The geomechanics classification in rock engineering applications. In: Proc. of the 4th ISRM Cong., Montreux, Suisse. Balkema, Rotterdam, pp 51–58

Bieniawski ZT (1989) Engineering rock mass classifications. Wiley, New York, p 251

Budetta P (2004) Assessment of rockfall risk along roads. Nat Hazards Earth Syst Sci 4:71–81

Budetta P, Panico M (2002) Il metodo "Rockfall Hazard Rating System" modificato per la valutazione del rischio da caduta massi sulle vie di comunicazione. G Geol Tecnica Ambient 4:3–13

Calcaterra D, De Luca Tupputi Schinosa F, Fenelli GB (2004) Rockfall hazard assessment at Mt. San Costanzo (Sorrento Peninsula, Italy). Landslides: evaluation and stabilization. Lacerda, Ehrlich, Fontoura & Sayo (eds) pp 265–271

Cancelli A, Crosta G (1993) Hazard and risk assessment in rockfall prone areas. In: Skipp BO (ed) Risk reliability in ground engineering, Thomas Telford, pp 177–190

Colangelo G, Guariglia A (2011) A combined methodology for landslide risk mitigation in Basilicata Region by using LIDAR technique and rockfall simulation. Int J Geophys 2011, 392676, 5 pp. doi:10.1155/2011/392676

Corominas J, Copons R, Moya J, Vilaplana JM, Altimir J, Amigò J (2005) Quantitative assessment of the residual risk in a rockfall protected area. Landslides 2:343–357

Cotecchia V, D'Ecclesiis G, Polemio M (1990) Studio geologico e idrogeologico dei monti di Maratea. Geologia Applicata e Idrogeologia, Vol. XXV, Bari

D'Argenio B, Pescatore TS, Scandone P (1973) Schema geologico dell'Appennino meridionale (Campania e Lucania). Atti Accad Naz Lincei Quad 183:49–72

De Almeida JA, Kullberg JC (2011) Rockfall hazard and risk analysis for Monte da Lua, Sintra, Portugal. Nat Hazards 58:289–310

Dorren LKA, Seijmonsbergen AC (2003) Comparison of three GIS-based models for predicting rockfall runout zones at a regional scale. Geomorphology 56:49–64

Ferlisi S, Cascini L, Corominas J, Matano F (2012) Rockfall risk assessment to persons travelling in vehicles along a road: the case study of the Amalfi coastal road (southern Italy). Nat Hazard 62:691–721

Franklin JA, Senior SA (1997) The Ontario rockfall hazard rating system. In: Proceedings of international conference on engineering geologu and environment, vol. 1, pp 647–656

Frattini P, Crosta G, Carrara A, Agliardi F (2008) Assessment of rockfall susceptibility by integrating statistical and physically-based approaches. Geomorphology 94:419–437

Geo&Soft (2004) Rotomap - Manualed'uso. http://www.geoandsoft.it

Ghosh S, Gunther A, Carranza EJM, Van Westen CJ, Jetten VG (2010) Rock slope instability assessment using spatially distributed structural orientation data in Darjeeling Himalaya (India). Earth Surface Processes and Landforms 35(15):1773–1792

Glade T, Anderson M, Crozier MJ (2005) Landslide hazard and risk. Wiley, New York, p 802

Gupta V, Tandon RS (2014) Kinematic rockfall hazard assessment along a transportation corridor in the Upper Alaknanda valley, Garhwal Himalaya. India Bull Eng Geol Environ. doi:10.1007/s10064-014-0623-7

Guzzetti F, Crosta G, Detti R, Agliardi F (2002) STONE: a computer program for the three dimensional simulation of rock-falls. Comput Geosci 28(9):1079–1093

Guzzetti F, Reichenbach P, Ghigi S (2004) Rockfall hazard and risk assessment along a transportation corridor in the Nera Valley, Central Italy. Environ Manag 34(2):191–208

INGV (2010) ISIDe- Italian Seismological Instrumental and parametric database. http://iside.rm.ingv.it

ISRM (1981) Suggested method for the quantitative description of discontinuities in rock masses. In: Brown ET (ed) Rock characterization testing and monitoring. Pergamon, Oxford, pp 3–52

Maeez NH, Youssef A (2004) Development of a highway rock cut rating system for Missouri highways. Development and technology.Missouri Department of Transportation, Jefferson

Markland JT (1972) A useful technique for estimating the stability of rock slopes when the rigid wedge sliding type of failure is expected. Imperial College Rock Mechanics Research Report No. 19, pp 10

Mauldon M, Drumm EC, Dunne WM, Bateman V, Rose B, Kim M (2007) Rockfall management system for Tenesse. Division of Materials and Tests, Tennessee Department of Transportation, Nashville

Mavrouli O, Corominas J (2010) Vulnerability of simple reinforced concrete buildings to damage by rockfalls. Landslides 7:169–180

Mignelli C, Lo Russo S, Peila D (2012) ROckfall risk Management assessment: the RO.MA. Nat Hazards 62:1109–1123

Pack R, Boie K, Mather S, Farrell J (2006) UDOT rockfall hazard rating system: final report and user's manual (Report UT-06.07). Utah State University, Logan

Pantelidis L (2011) A critical review of highway slope instability risk assessment systems. Bull Eng Geol Environ 70:395–400

Pellicani R, Van Westen CJ, Spilotro G (2014a) Assessing landslide exposure in areas with limited landslide information. Landslides 11(3):463–480. doi:10.1007/s10346-013-0386-4

Pellicani R, Frattini P, Spilotro G (2014b) Landslide susceptibility assessment in Apulian Southern Apennine: heuristic vs. statistical methods. Environ Earth Sci 72(4):1097–1108. doi:10.1007/s12665-013-3026-3

Pfeiffer T, Bowen T (1989) Computer simulation of rock falls. Bull Assoc Eng Geol 26(1):135–146

Pierson LA, Van Vickle R (1993) Rockfall hazard rating system—participant's manual. SNI International Resources Inc., Phoenix

Pierson LA, Davis SA, Van Vickle R (1990) Rockfall hazard rating system implementation manual. Report FHWA-OR-EG-90-01, Federal Highway Administration (FHWA), U.S. Department of Transportation, Washington

Piteau DR, Clayton R (1978) Computer rockfall model. Proceedings meeting on rockfall dynamics and protective works effectiveness, Bergamo, Italy, ISMES, 90: 123–125

Rizzo V, Leggeri M (2004) Slope instability and sagging reactivation at Maratea (Potenza, Basilicata, Italy). Eng Geol 71:181–198

Romana M (1985) New adjustment rating for application of Bieniawski classification to slopes. Int. Symp. Role of Rock Mechanics. Zacatecas. pp 49–53

Russel CP, Santi P, Humphrey JD (2008) Modification and statistical analysis of the Colorado rockfall hazard rating system. Colorado School of Mines, Golden

Scioldo G (2006) User guide ISOMAP & ROTOMAP—3D surface modelling and rockfall analysis. Geo&Soft International, Torino

Spilotro G, Petraglia A, Pizzo V (2004) Strada Statale n.18 "Tirrena Inferiore". Assistenza tecnica per l'acquisizione ed il trattamento dei dati necessari alla zonazione della pericolosità e del rischio di caduta massi lungo il tratto di strada compreso tra i km 220 + 600 e 243 + 670. Relazione generale. ANAS – Ente Nazionale per le strade- Compartimento Regionale della Viabilità - Potenza

Stock GM, Luco N, Collins BD, Harp EL, Reichenbach P, Frankel KL (2012) Quantitative rock-fall hazard and risk assessment for Yosemite Valley, Yosemite National Park, California. USGS Scientific Investigations Report 2014–5129. http://pubs.usgs.gov/sir/2014/5129/

Stoffel M, Wehrli A, Kuhne R, Dorren LKA, Perret S, Kienholz H (2006) Assessing the protective effect of mountain forests against rockfall using a 3D simulation model. For Ecol Manag 225:113–122

Topal T, Akin MK, Akin M (2012) Rockfall hazard analysis for an historical Castle in Kastamonu (Turkey). Nat Hazards 63(3):255–274

Turner AK, Schuster RL (2013) Rockfall: characterization and control. Transportation Research Board, Washington, **658p**

Varnes DJ (1984) Landslide hazard zonation: a review of principles and practice. United Nations International, Paris

Volkwein A, Schellenberg K, Labiouse V, Agliardi F, Berger F, Bourrier F, Dorren LKA, Gerber W, Jaboyedoff M (2011) Rockfall characterization and structural protection—a review. Nat Hazards Earth Syst Sci 11:2617–2651

Wang X, Frattini P, Crosta GB, Zhang L, Agliardi F, Lari S, Yang Z (2013) Uncertainty assessment in quantitative rockfall risk assessment. Landslides. doi:10.1007/s10346-013-0447-8

Yilmaz I, Yildirim M, Keskin I (2008) A method for mapping the spatial distribution of *RockFall* computer program analyses results using *ArcGIS* software. Bull Eng Geol Environ 67:547–554

Youssef AM, Maerz NH (2012) Development, justification, and verification of a rock fall hazard rating system. Bull Eng Geol Environ 71:171–186

R. Pellicani (✉) · G. Spilotro
Department of European and Mediterranean Cultures,
University of Basilicata,
Matera, Italy
e-mail: roberta.pellicani@unibas.it

C. J. Westen
Faculty of Geo-information Sciences and Earth Observation,
University of Twente,
Enschede, The Netherlands